MODELING PLANKTON PRODUCTION IN THE EASTERN MEDITERRANEAN: APPLICATION OF A 1-D VERTICALLY-RESOLVED PHYSICAL-BIOLOGICAL MODEL TO THE IONIAN AND RHODES BASINS

ERNESTO NAPOLITANO[1], TEMEL OGUZ[2],
PAOLA MALANOTTE-RIZZOLI[3], EMILIO SANSONE[1]

[1] *Institute of Meteorology and Oceanography, Istituto Universitario Navale, Naples, ITALY*
[2] *Middle East Technical University, Institute of Marine Sciences, Erdemli 33731, Icel, TURKEY*
[3] *Massachusettes Institute of Technology, Department of Earth, Atmospheric and Planetary Sciences, Cambridge, 02139, MA, USA .*

Abstract A one dimensional, coupled physical-biological model is used to study the biological production characteristics of the Rhodes and western Ionian basins of the Eastern Mediterranean. The biological model involves single aggregated compartments of phytoplankton, zooplankton, detritus as well as ammonium and nitrate forms of the inorganic nitrogen. The model simulations point to the importance of the contrasting dynamical characteristics of these two basins on affecting their yearly planktonic structures. The western Ionian basin is shown to possess only 10% of the Rhodes' productivity and therefore represent a most oligotrophic site in the Eastern Mediterranean. The Rhodes basin reveals a strong bloom in early spring, typically in March, a weaker bloom in early winter, typically in January, and a subsurface production below the seasonal thermocline during summer. This structure is slightly modified in the western Ionian basin, and the early winter and early spring blooms are merged to cover the entire winter. These results are supported favorably by the available observations both in their magnitudes and timing.

P. Malanotte-Rizzoli and V.N. Eremeev (eds.),
The Eastern Mediterranean as a Laboratory Basin for the Assessment of Contrasting Ecosystems, 181–204.

1. Introduction

In terms of its biochemical characteristics, the Eastern Mediterranean tends to be a poorly studied basin. Observations are confined generally to coastal areas as very little data are available for its offshore waters. The three dimensional, three compartment model by Crise et al (1998; hereafter referred to as CCM, 1998a) and Crispi et al. (1998; hereafter referred to as CCM, 1998b) is the only modeling work carried out insofar. This model investigates primarily the response of the circulation dynamics on the identification of different oligotrophic regimes of the Mediterranean sub-basins. When compared with the CZCS imagery, it seems to reproduce observed chlorophyll distributions according to the prevailing cyclonic and anticyclonic flow regimes.

The models with simplified biology using a limited number of state variables (usually four or five) are useful tools providing possible representation of pelagic ecosystem and its interactions with the upper layer dynamics. They have been applied successfully to different oceanic regimes (e.g. Fasham et al., 1991; McGillicuddy et al., 1995; McClain, 1995; Doney et al., 1996; Oguz et al., 1996; Kuhn and Radach, 1997). In this paper, we describe the characteristics of biological production of the Rhodes and the Ionian basins of the Eastern Mediterranean using such a simplified model. The Ionian and Rhodes basins are chosen particularly since they reflect two constrasting ecosystems; while the former represents a typical oligotrophic environment, the latter is known to be one of the most productive region of the Mediterranean Sea. These two basins also differ substantially by their dynamical regimes which govern ultimately their ecosystem characteristics.

The Rhodes cyclonic gyre is the most persistent feature of the Levantine basin circulation located in the northern Levantine basin to the west of Cyprus. Its dynamical and chemical characteristics are reasonably well-explored by a series of systematic surveys of the R.V. Bilim during the last decade (Salihoglu et al., 1990; Ozsoy et al., 1991, 1993; Sur et al., 1992; Yilmaz et al., 1994; Ediger and Yilmaz, 1996; Ediger et al., 1998; Yilmaz and Tugrul, 1998). On the other side, the Ionian Sea, identified as the region from the Sicily Strait to the Cretan passage, is a transition basin across which different water masses (e.g. Modified Atlantic Water, MAW; Levantine Intermediate water, LIW; Eastern Mediterranean Deep Water, EMDW) undergo transformations along their pathways between the Eastern and Western Mediterranean (Malanotte-

Rizzoli, et al., 1997). Here, we restrict our attention only to the western Ionian Sea characterized by the anticyclonic circulation and by the least dense upper layer water mass of the Eastern Mediterranean, MAW. It, therefore, offers completely opposite characteristics to those found in the Rhodes gyre. Practically, we perform here an intercomparision study to explore the biological characteristics of two regions known qualitatively as the most productive and the most oligotrophic sites of the Eastern Mediterranean and to relate them to the prevaling regional physical and dynamical characteristics. The paper is organized as follows. A brief description of the model formulation is first provided in Section 2. Its applications to the Rhodes and Ionian basins are then given in Sections 3 and 4, respectively. Conclusions are given in Section 5.

2. Model Description

The model is similar to the one described by Oguz et al. (1996) for studying the Black Sea annual plankton dynamics. It is a coupled physical-biological model including the level 2.5 Mellor and Yamada turbulence parameterization for vertical mixing. The biological state variables considered are phytoplankton biomass P, herbivorous zooplankton biomass H, and labile pelagic detritus D. Nitrate N and ammonium A constitute the other two state variables, since recent findings of relatively low N/P ratios (with respect to its Redfield value) in the euphotic zone of the northern Levantine imply nitrogen as the limiting nutrient for the primary production in the Rhodes gyre region (Ediger, 1995; Yilmaz and Tugrul, 1998).

The local changes of the biological variables are expressed by a time and depth dependent advection-diffusion equation for transport, source and sinks in a one dimensional vertical water column. The general form of the equation is given by

$$\frac{\partial B}{\partial t} = \frac{\partial}{\partial z}\left[(K_h + \nu_h)\frac{\partial B}{\partial z}\right] + F_B \qquad (1)$$

where B represents any of the five biological variables, t is time, z is the vertical coordinate, ∂ denotes the partial differentiation. F_B represents the biological interaction terms expressed for the phytoplankton, herbivore, detritus,

ammonium, and nitrate equations, respectively, as

$$F_P = \Phi(I,N,A)\,P - G(P)\,H - m_p P \tag{2}$$

$$F_H = \gamma G(P)\,H - m_h H - \mu_h H \tag{3}$$

$$F_D = (1-\gamma)\,G(P)\,H + m_p P + m_h H - \epsilon D + w_s \frac{\partial D}{\partial z} \tag{4}$$

$$F_A = -\Phi_a(I,A)\,P + \mu_h H + \epsilon D - \Omega A \tag{5}$$

$$F_N = -\Phi_n(I,N)\,P + \Omega A \tag{6}$$

where the definition of parameters and their values used in the experiments are given in Table 1. The functions $\Phi(I,N,A)$ and $G(P)$ denote the light and nutrient limited phytoplankton growth and zooplankton grazing, respectively. The latter is represented by the maximum ingestion rate σ_g multiplied by the Michaelis-Menten type limitation function

$$G(P) = \sigma_g \frac{P}{R_g + P} \tag{7}$$

where R_g is the half saturation constant for the zooplankton grazing. Eq. (7) implies that zooplankton graze only phytoplankton. Their grazing on the detrital material is not taken into account since this usually constitutes only a small fraction of zooplankton diet (about 10%).

The phytoplankton production is parameterized as product of the maximum growth rate σ_m, minimum of the light and nutrient limitation functions and the phytoplankton standing crop. The temperature limitation of the phytoplankton growth is not included in the model, for simplicity. Then, the net growth rate $\Phi(I,N,A)$ is given by

$$\Phi(I,N,A) = \sigma_m min\left[\alpha(I), \beta_t(N,A)\right] \tag{8}$$

where min refers to the minimum of either the light limitation function $\alpha(I)$ or the total nitrogen limitation function $\beta_t(N,A)$. The latter is expressed as the sum of ammonium and nitrate limitation functions, $\beta_a(A)$ and $\beta_n(N)$, respectively

$$\beta_t(N,A) = \beta_n(N) + \beta_a(A) \tag{9}$$

They are given by the Michaelis-Menten type uptake formulation as

$$\beta_a(A) = \frac{A}{R_a + A}, \qquad \beta_n(N) = \frac{N}{R_n + N}\exp(-\psi A) \tag{10}$$

where R_n and R_a are the half-saturation constants for nitrate and ammonium, respectively. The exponential term in eq. 10 represents the inhibiting effect of ammonium concentration on nitrate uptake, with ψ signifying the inhibition parameter.

Table 1. Model parameters used in the numerical experiments

Parameter	Definition	Value Rhodes	Value Ionian	Unit
a	Photosynthesis efficiency parameter	0.01	0.02	m^2W^{-1}
k_w	Light extinction coefficient for PAR	0.05	0.04	m^{-1}
k_c	Phytoplankton self-shading coefficient	0.04	0.07	m^2 (mmol N)$^{-1}$
σ_p	Maximum phytoplankton growth rate	1.5	1.0	day^{-1}
m_p	Phytoplankton mortality rate	0.04	0.04	day^{-1}
σ_g	Zooplankton maximum grazing rate	0.6	0.8	day^{-1}
m_h	Zooplankton mortality rate	0.04	0.04	day^{-1}
μ_h	Zooplankton excretion rates	0.07	0.04	day^{-1}
γ_h	Food assimilation efficiency	0.75	0.75	Dimensionless
R_n	Half saturation constant in nitrate uptake	0.5	0.5	mmol N m^{-3}
R_a	Half saturation constant in ammonium uptake	0.2	0.2	mmol N m^{-3}
R_g	Half saturation constant for zooplankton grazing	0.5	0.5	mmol-N m^{-3}
ψ	Ammonium inhibition parameter of nitrate uptake	3	3	(mmol N m^{-3})$^{-1}$
ϵ	Detritus decomposition rate	0.1	0.1	day^{-1}
w_s	Detrital sinking rate	8.0	5.0	m day^{-1}
Ω_a	Nitrification rate	0.05	0.05	day^{-1}
ν_b	Background kinematic diffusivity	0.1	0.1	cm^2s^{-1}

The individual contributions of the nitrate and ammonium uptakes to the phytoplankton production, given in eq's (5) and (6), are represented respectively by

$$\Phi_n(I,N) = \Phi(I,N,A)\left(\frac{\beta_n}{\beta_t}\right), \qquad \Phi_a(I,A) = \Phi(I,N,A)\left(\frac{\beta_a}{\beta_t}\right) \tag{11}$$

The light limitation is parameterized according to Jassby and Platt's (1976)

hyperbolic tangent function and exponentially decaying irradiance with depth as

$$\alpha(I) = tanh[aI(z,t)] \tag{12}$$

$$I(z,t) = I_s \exp[-(k_w + k_c P)\, z] \tag{13}$$

where a denotes photosynthesis efficiency parameter controlling the slope of $\alpha(I)$ versus the irradiance curve at low values of the Photosynthetically Active Radiance (PAR). I_s denotes the surface intensity of PAR taken as the half of the climatological incoming solar radiation. k_w is the light attenuation coefficient due to sea water, and k_c is the phytoplankton self-shading coefficient. In the above formulation, k_w and k_c are taken to be constant with depth. The daily variation of the light irradiance, and hence the phytoplankton growth are neglected since the biological processes we consider have time scales much longer than a day.

2.1. Boundary Conditions

No-flux conditions described by

$$(K_h + \nu_h)\frac{\partial B}{\partial z} = 0 \tag{14}$$

are specified both at the surface and the bottom boundaries of the model for the variables P, H, N, and A. For detritus, it is modified to include the contribution of downward sinking flux

$$(K_h + \nu_h)\frac{\partial D}{\partial z} + w_s D = 0 \tag{15}$$

The bottom boundary of the model is taken at the 400 m depth for the Rhodes case and at the 300 m depth for the Ionian case, which are well below the euphotic zone comprising only the upper 100 m of the water column. Considering our choice of moderate detritus sinking rates (see Table 1), the advantage of locating the bottom boundary at considerable distance away from the euphotic layer is to allow complete remineralization of the detrital material until it reaches the lower boundary of the model. The complete remineralization was ensured by setting appropriate decomposition rate of detrital material in the model. This approach avoids prescription of the non-zero flux boundary condition in order to compensate the loss of detritus (if any) to the deep interior from the boundary. It is thus implicitely assumed here that the detrital pool

in the model is formed by smaller size particles. Fast sinking large particles with a typical speed of the order of 100 m/day are therefore not modeled in the present work. We note that equations (2)-(6) together with the boundary conditions (14) and (15) provide a closed, fully conserved system. The state of the system at time t is governed solely by internal dynamical processes without any contribution from the external sources.

The physical model is forced by daily climatological atmospheric fluxes. The wind stress forcing are taken from the ECMWF climatology. The heat flux data are provided by May (1982) whereas the data given by Antoine, Morel and Andre (1995) for the Ionian Sea is used for the specification of PAR for both simulations. The heat flux data is, however, adjusted slightly to provide the zero annual mean over the year. This adjustment is necessary to avoid the drift of the model from its perpetual state due to continuous warming/cooling of the water column during the time integration of the temperature equation. The resulting adjusted heat flux distributions over the year are shown in Fig. 1. The Rhodes basin receives greater cooling in winter (~200 W/m^2) as compared to the value of 130 W/m^2 for the Ionian Sea. In the summer, the warming in the Rhodes basin reaches 180 W/m^2 which is also higher from that of the Ionian basin by about 40 W/m^2. PAR attains its maximum intensity of 140 W/m^2 during the summer months, whereas its minimum value is set to 40 W/m^2 during December and January. Instead of prescribing the fresh water flux at the surface, the model is forced by the surface salinity whose annual variations are specified by the Mediterranean Oceanic Data Base (MODB) data set (Brasseur et al., 1996). The forcing by surface salinity instead of the fresh water flux using evaporation minus precipitation data is a matter of convinience here since it provides more realistic yearly salinity variations in the near-surface levels of the water column.

Although the atmospheric forcing functions used in the model are rather idealized, they are adequate for the purpose of the present work since the surface layer dynamics is introduced to the biological model only indirectly by specification of the vertical eddy diffusivity. There is no other feed back mechanism between the physical and biological models. The vertical eddy diffusion coefficient of the biological model is same with that of temperature or salinity computed from the turbulence closure parameterization (see Oguz et al., 1996 for details).

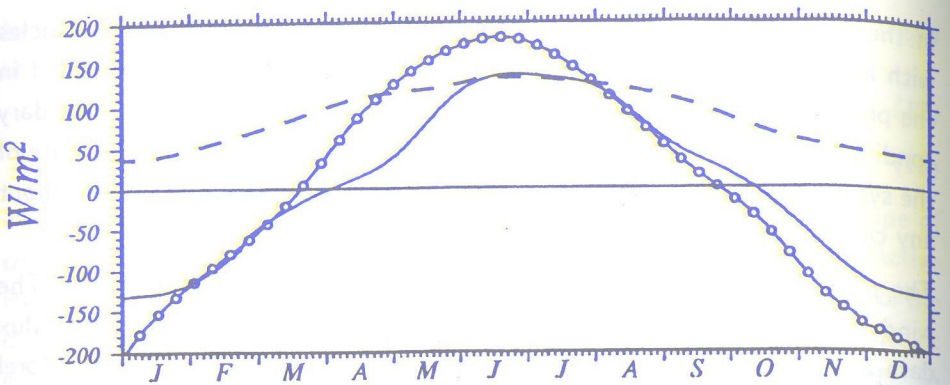

Figure 1: *Climatological daily averaged heat fluxes; continuous line is for the Ionian basin, continuous line with open circles for the Rhodes basin, and photosynthetically available radiation (broken line) used in the simulation. Units are in* Wm^{-2}

2.2. Initial Conditions

The model is initialized with the stably stratified upper ocean temperature and salinity profiles representative of the summer/autumn climatological conditions (Fig. 2a). The same initial temperature profile is used for both Rhodes and Ionian simulations since the subsurface structures of these two regions reflect characteristics of the LIW below 100-150 m depth. The salinity, on the other side, differs greatly between these two basins. The upper 150 m of the water column in the Rhodes gyre is occupied by much more saline water mass (with S>39.0 ppt) as compared to less saline modified Atlantic-based waters (minimum S$\sim$ 37.4 ppt) in the western Ionian basin (Fig. 2a).

In the biological model, the initial nitrate source drives the system as they are entrained and diffuse upward and utilized ultimately for the biological production. In the absence of any external source and sink as implied by the boundary conditions (see eq.'s 14 and 15), the model simply redistributes the initial nitrate source among the living and nonliving components of the system. Thus, specification of the initial phytoplankton, zooplankton, detritus and ammonium distributions is unimportant as they will be generated by the model during its transient evolution. The initial subsurface nitrate structure however will govern, to a large extent, the level of productivity in the euphotic zone. Accordingly, the state variable except nitrate are initialized by a vertically uniform small, non-zero values within the euphotic layer for both cases. The initial vertical nitrate structures are specified according to the data given by Berland et al. (1988) and Yilmaz and Tugrul (1998). These observed profiles, shown in Fig. 2b, demonstrate quite clearly how these two basins differ substantially in terms of their subsurface nitrate structure below the 100m depth. The Rhodes gyre reveals vertically uniform subsurface nitrate concentrations on the order of 5 μM. On the other side, the western Ionian subsurface nitrate concentrations increase more gradually with depth and reach the similar nitrate level of the Rhodes basin only below 500 m depth. As it will be presented in the following sections, these differences in the nitrate and salinity structures play crucial roles on the ultimate biological characteristics of these two regions.

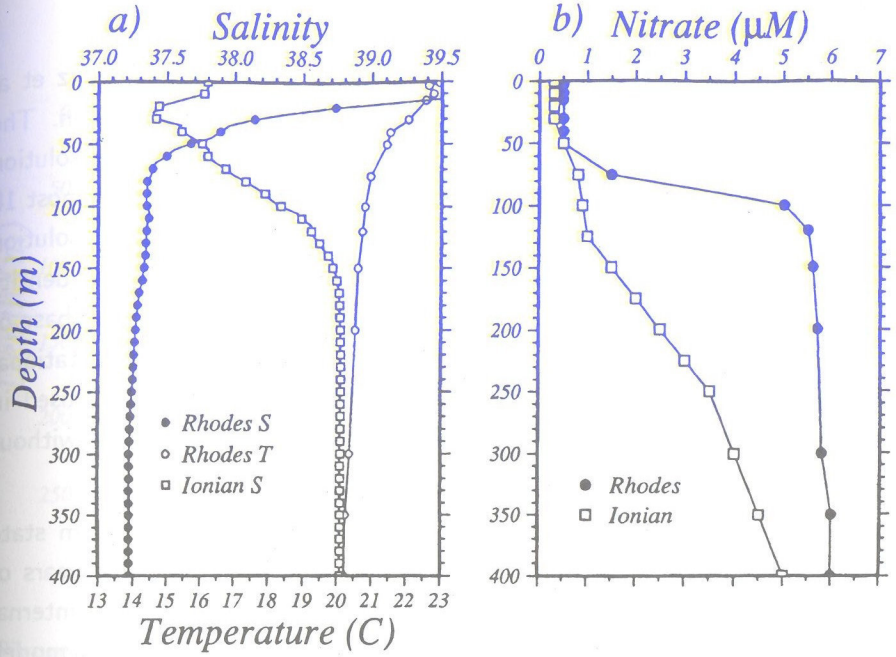

Figure 2: *The profiles of (a) temperature and salinity, and (b) nitrate used for the model initializations*

2.3. Numerical Procedure

The numerical solution of the model equations are described in Oguz et al (1996). A total of 51 vertical levels is used to resolve to water column. The grid spacing is compressed slightly towards the surface to increase the resolution within the euphotic zone. Accordingly, the vertical grid spacing is at most 10 m for the Rhodes case and about 7 m for the Ionian case. This resolution is found to be quite adequate to represent properly steep gradients of density and nitrate between the seasonal thermocline/pycnocline and the the base of the euphotic zone. The numerical scheme is implicit to avoid computational instabilities due to small grid spacing. A time step of 5 minutes, used in the numerical integration of the equations, provides a stable solution without introducing numerical noise.

First, the physical model is integrated for five years. An equilibrium state with repeating yearly cycle of the dynamics is achieved after three years of integration in response to the imposed external forcings and to the internal processes in the system. Using the results of the fifth year of the physical model, the biological model is then integrated for four years to obtain repetative yearly cycles of the biological variables. The results of the biological model presented here are based on the fourth year of integration.

3. Simulation of Rhodes Basin ecosystem

3.1. Annual plankton structure

In agreement with its vertical mixing and stratification characteristics, the water column nitrate structure undergoes considerable variations during the year (Fig. 3a). The mixed layer waters of the entire summer and autumn seasons are extremely poor in nutrients, and characterized by only trace level nitrate concentrations of about 0.1 mmol/m^3. The nitrate depletion arises due to lack of supply from the subsurface levels because of the presence of strong seasonal thermocline/pycnocline. The zone of high stratification below the seasonal thermocline coincides with the strong nitrate variations (the so-called the nitracline). Approximately below 80-90 m depths, the nitrate attains its

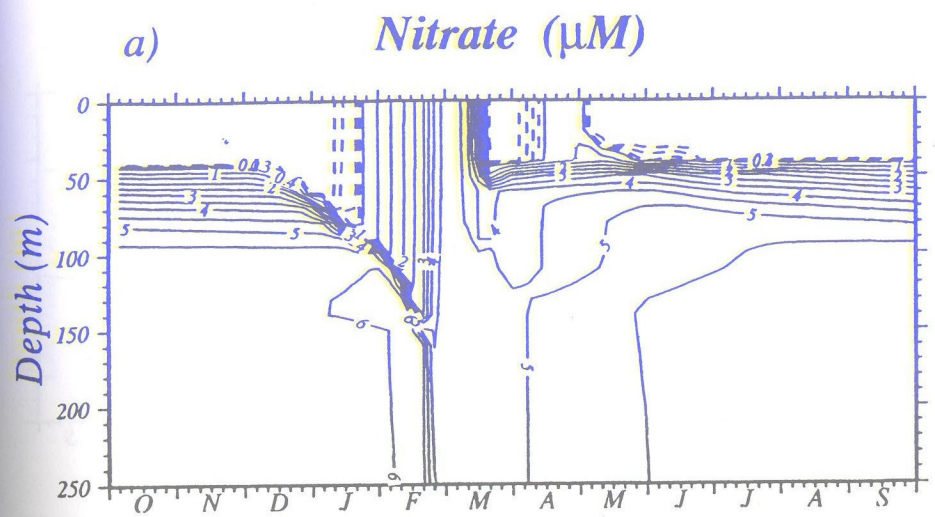

Figure 3: *Simulated annual distributions of (a) nitrate, (b) phytoplankton, (c) zooplankton, (d) detritus, (e) ammonium, within the upper 150 m depth for phyto- and zooplankton and the upper 250 m depth for others. Units are in μM. For nitrate, continuous lines are contours at intervals of 0.5 μM and broken lines at intervals of 0.1 μM. In all plots the time axis starts at October 1 and ends at September 30*

typical deep water values in excess of 5.0 mmol/m^3. This structure undergoes substantial modification during the winter months as the convective overturning mechanism brings the nitrate rich subsurface waters to near-surface levels. Under such conditions, nitrate concentrations attain their maximum values of 4.5 mmol/m^3 over the 400m deep homogeneous water column in February.

The phytoplankton structure exhibits a major algae production during the first half of March (Fig. 3b) immediately after the cessation of the strong mixing, shallowing of the mixed layer and higher rate of solar irradiance penetrating to deeper levels. Since the water column was already replenished by nitrate, all

b) **Phytoplankton (μM)**

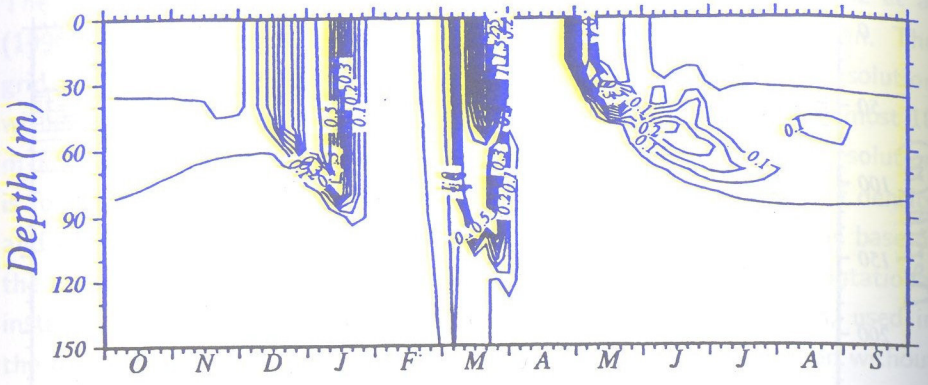

c) **Zooplankton (μM)**

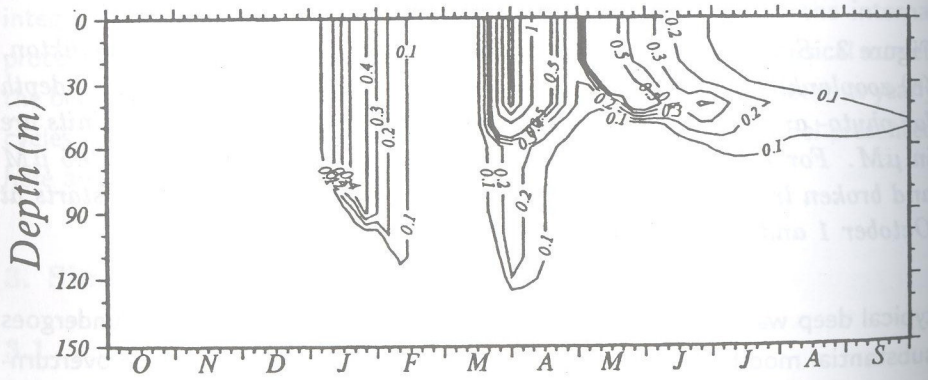

d) **Detritus (μM)**

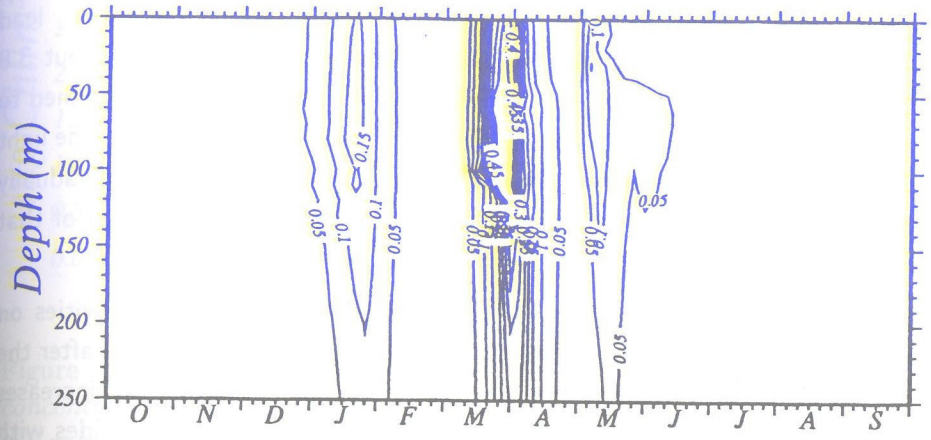

e) **Ammonium (μM)**

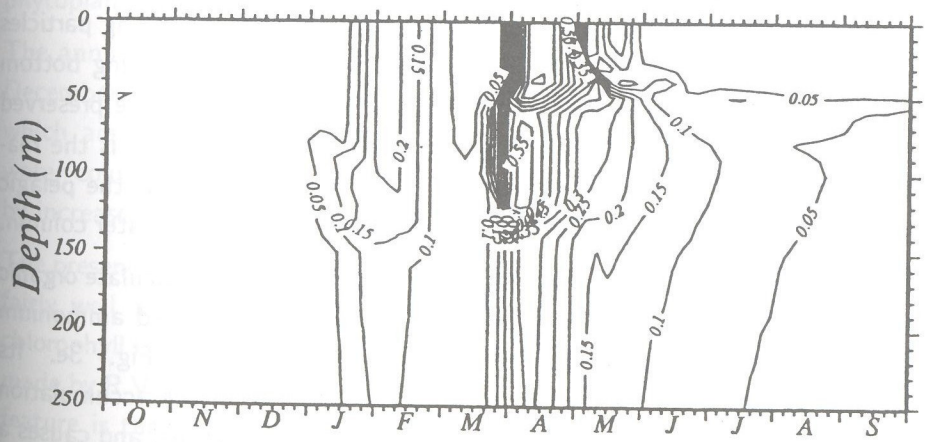

these conditions favor phytoplankton bloom, shown in Fig. 3b as an exponential increase of algae concentrations during the second week of March. High nitrate concentrations, built up in the water column during the winter, lead to generation of a very intense bloom with maximum biomass of about 3.8 mmol/m^3. It extends to the depth of 120 m, but its major part is confined to the upper 65 m because of the increasing role of self-shading effect on the light limitation. Following a week-long intense period, the bloom weakens gradually within the last week of March and terminates completely by the end of that month.

The early spring phytoplankton bloom initiates other biological activities on the living and non-living components of the pelagic ecosystem. Soon after the termination of the phytoplankton bloom, mesozooplankton biomass increases up to 2.2 mmol/m^3 during April (Fig. 3c). This period also coincides with increased detritus and ammonium concentrations (Fig. 3d,e) supported by excretion and mortality of phytoplankton and mesozooplankton communities. The major detritus accumulation in the water column in fact proceeds termination of phytoplankton bloom at begining of April. Moreover, sinking particles are remineralized completely within the upper 300 m before reaching bottom of the model at 400 m depth. All the detrital material is therefore preserved within the water column without any loss from the system. This is the reason for which the bottom boundary was taken at 400 m whereas the pelagic planktonic processes are confined within the upper 100 m of the water column.

The role of remineralization responsible for transforming the particulate organic nitrogen to inorganic dissolved nitrogen is indicated by increased ammonium concentrations up to 0.7 mmol/m^3 in March-April period in Fig. 3e. Its eventual oxidation due to nitrification process leads to nitrate accumulation primarily in the mixed layer and to a less extent in the nitracline, and causes a short-term increase in phytoplankton biomass up to about 0.5 mmol/m^3 within the mixed layer during the first half of May (Fig. 3b). As in the previous case, this secondary bloom is also followed by a small increase in mesozooplankton biomass, as well as in detritus and ammonium concentrations. The surface-intensified phytoplankton bloom event continues below the seasonal thermocline for another month by consuming available nitrate and ammonium within the nitracline zone. The subsurface biomass diminishes gradually towards the end of July as the contribution of losses from mesozooplankton grazing and

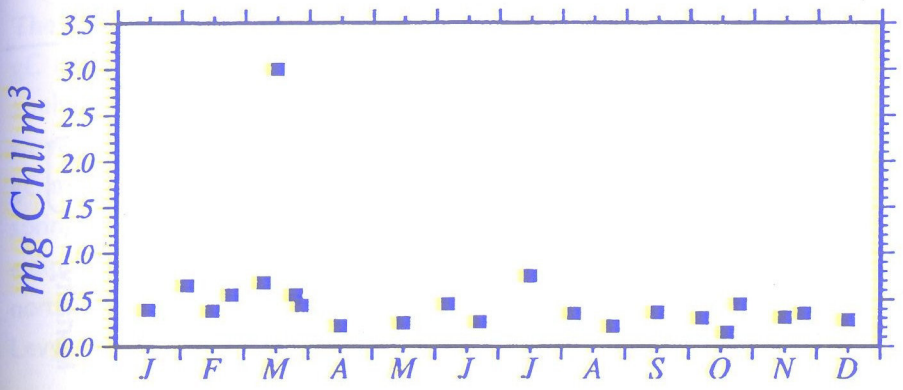

Figure 4: *A composite picture of the euphotic layer average chlorophyll concentrations (in mg Chl/m^3) within the year. The data compiled from the measurements of R.V. Bilim in the Rhodes gyre region during 1986-1995 period (A. Yilmaz, private com.)*

phytoplankton mortality exceeds production.

The annual phytoplankton structure exhibits another weak bloom from mid-December to mid-January. This is associated with the consumption of nitrate which are made readily available by the convective mixing initiated in the water column with the begining of cooling season. Once again, it is followed by increase in mesozooplankton stocks in January-February.

The presence of early spring bloom and other features of the model is supported fairly well by the observations. Fig. 4 shows the euphotic layer-averaged chlorophyll concentrations in the Rhodes gyre based on the data from 23 casts made by R.V. Bilim during the last 10 years. In this figure, the most noticeable feature is the chlorophyll value of 3.0 mg Chl/m^3 during March comparable with the values simulated from the model.

3.2. Annual Budget and Primary Production estimates

The annual mean intercompartmental transfer rates over the euphotic zone and the vertical fluxes across its base are shown in Fig. 5. They are expressed in terms of gC m^{-2} yr^{-1} and obtained by multiplying all the fluxes computed

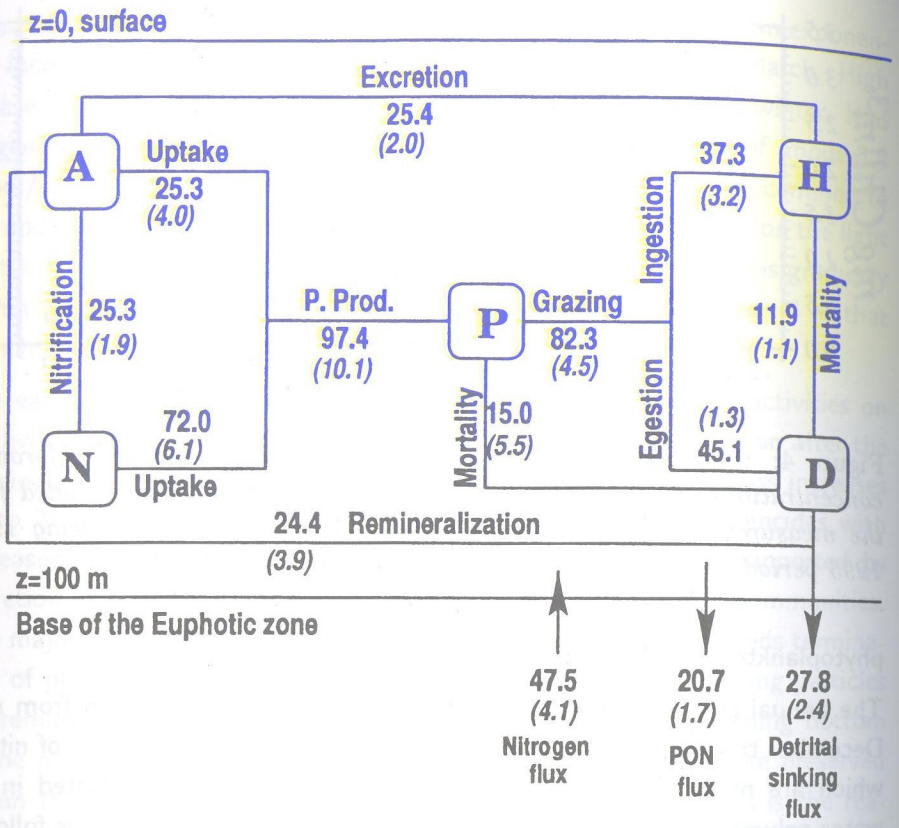

Figure 5: *The annual nitrogen budget of the euphotic zone for both Rhodes and Ionian simulations. The latter is shown by the numbers in parantheses*

in *mmol* nitrogen units by the factor 0.12. At the base of the euphotic zone, the budget implies that the vertical diffusive nitrogen flux of 47.5 gC m^{-2} yr^{-1} from below is balanced by the sum of downward PON flux of 20.7 gC m^{-2} yr^{-1} and detrital sinking flux of 27.8 gC m^{-2} yr^{-1} leaving the euphotic zone. The total primary production (PP) is estimated as 97.4 gC m^{-2} yr^{-1} whose 25 % is met by ammonium uptake and the rest by the nitrate uptake. We, however, note that only two-third of the overall nitrate uptake of 72.0 gC m^{-2} yr^{-1} is supported from the subsurface levels and accounts for the new production, the rest is accounted by the recycling mechanism inside the euphotic zone. The budget suggests approximately 40% of the PP (37.3 gC m^{-2} yr^{-1}) is utilized for the secondary production, whereas the rest goes directly into the detrital pool.

The PP estimation of 97 gC m^{-2} yr^{-1} agrees well with the value of 86.8 gC m^{-2} yr^{-1} computed by Antoine et al. (1995) on the basis of the CZCS analyses for the Northern Levantine. Using the data from 1986 and 1987 surveys of R.V. Bilim, Salihoglu et al. (1990) suggested a lower value of 60 gC m^{-2} yr^{-1}. This estimate however does not cover the data from productive spring period, and therefore underestimates the annual rate. Moreover, our estimate is comparable with the value of 105 gC m^{-2} yr^{-1} obtained for the northwestern Mediterranean characterized by similar dynamical conditions (c.f. Levy et al., 1998).

4. Simulation of Ionian Basin ecosystem

Similar to their physical characteristics, a substantial difference in the water column nitrate structure of the western Ionian and Rhodes basins is indicated by Fig. 6a. The weak vertical mixing in the winter months imply lack of sufficient nitrate supply from the subsurface levels to support the biological production in the subsequent early spring season. Fig. 6a clearly shows no nitrate accumulation inside the mixed layer during the winter. Whatever nitrate is entrained into the mixed layer from the subsurface levels is consumed immediately in the phytoplankton production process. This is initiated during mid-January and gradually increased to its peak at the end of February (Fig. 6b). The phytoplankton biomass can attain in this period only 0.25 mmol N/m^3 which is an order of magnitude lower than the typical spring bloom values of the Rhodes simulation. The degradation of the phyoplankton bloom occurs during March. April is the period of intense nitrogen cycling followed by surface-intensified regenerated production during early May and its continuation at the subsurface levels below the thermocline in June with the maximum biomass of 0.16 mmol/m^3. The response of subsurface production can be traced in the nitrate field by the slight increase of isolines during early summer period (Fig. 6a). The annual distribution of zooplankton stock (Fig. 6c) reveals maximum biomass value of about 0.15 mmol/m^3 within the year. This is again one order of magnitude smaller than the values given in the Rhodes simulations.

The way in which the intensity of vertical mixing controls timing of the early spring phytoplankton bloom was described earlier in Oguz et al. (1996) in

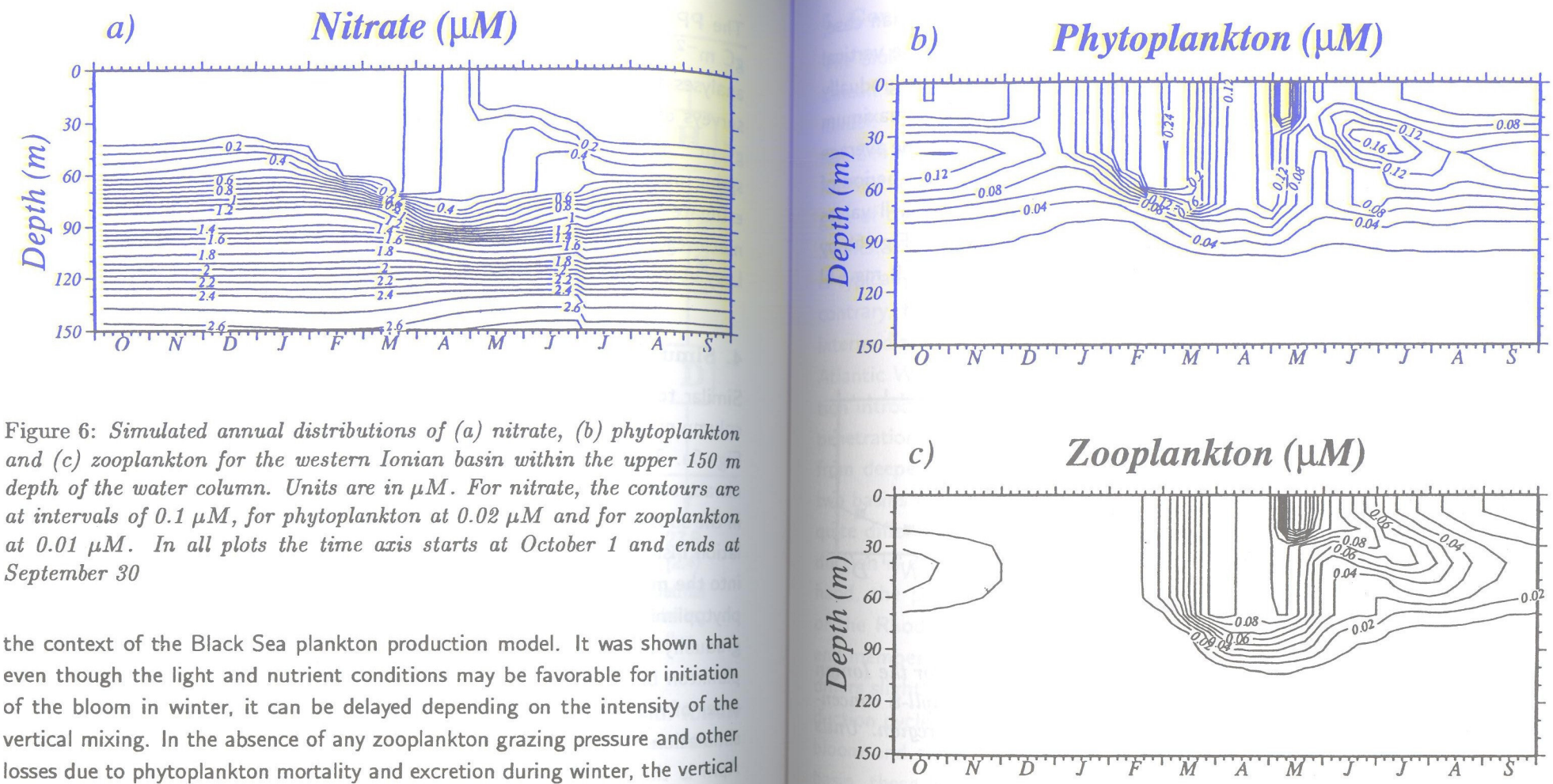

Figure 6: *Simulated annual distributions of (a) nitrate, (b) phytoplankton and (c) zooplankton for the western Ionian basin within the upper 150 m depth of the water column. Units are in μM. For nitrate, the contours are at intervals of 0.1 μM, for phytoplankton at 0.02 μM and for zooplankton at 0.01 μM. In all plots the time axis starts at October 1 and ends at September 30*

the context of the Black Sea plankton production model. It was shown that even though the light and nutrient conditions may be favorable for initiation of the bloom in winter, it can be delayed depending on the intensity of the vertical mixing. In the absence of any zooplankton grazing pressure and other losses due to phytoplankton mortality and excretion during winter, the vertical mixing is the only sink term which can balance the production. The initiation of phytoplankton bloom therefore depends on the relative intensities of these two terms during winter-early-spring period. The biological production will therefore be initiated whenever the vertical mixing weakens and its magnitude is exceeded by that of the production term. In our simulations, the Rhodes case is a good example for the delay of the bloom until the weakening of the intense mixing event taking place during the winter. The other region having similar features is the northwestern Mediterranean deep water formation area where prevention of the bloom by strong vertical mixing was referred to as

"deep mixing limitation of the bloom" (Levy et al., 1998). The Ionian case, on the contrary, favors biological conditions weakly-controlled by the vertical mixing. Thus, the bloom initiates earlier in winter and intensifies gradually until the net limitation factor $\Phi(I, N, A)$ given by eq. 8 attains its maximum value. The monthly mean CZCS chlorophyll data (Fig. 7), given as the average of pixels inside our analysis area, seem to support such an extended period of increased phytoplankton activity. The magnitude of CZCS chlorophyll values also compare well with the surface phytoplankton biomass values in Fig. 6b by using a conversion factor of 1 mmol nitrogen being equivalent to 1.2 mg Chl as before.

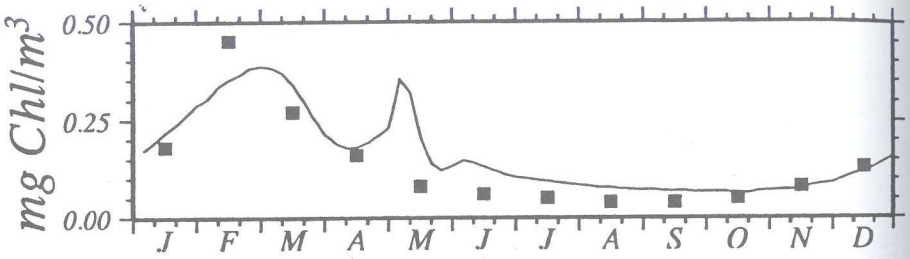

Figure 7: *Simulated annual surface chlorophyll-a distribution for the Ionian case (continuous line) and the CZCS-derived surface chlorophyll-a concentrations averaged from the pixels for the western Ionioan gyre region. Units are in mg Chl/m^3*

The annual budget and intercompartmental transfer rates for the Ionian simulation is also shown in Fig. 5 with the numbers in parantheses. The budget indicates that only 4.1 gC m^{-2} yr^{-1} nitrate flux enters into the euphotic zone from the lower layers. The contribution of recycled nitrogen through detrital breakdown and plankton excretion are 3.9 and 2.0 gC m^{-2} yr^{-1}, respectively, which all together give rise to a total PP rate of 10.1 gC m^{-2} yr^{-1}. This is an extremely low value, but is considered to be a typical for oligotrophic sites of the Eastern Mediterranean. Applying the CCM (1998a,b) model to the same region for the interpretation and analysis of the hydrographic and nutrient data collected during October 1991 and April 1992 surveys, Civitarese et al. (1996) obtained a very close mean PP value of 11.5 gC m^{-2} yr^{-1}.

5. Conclusions

The biological productivity in two contrasting regions of the Eastern Mediterranean is studied using a one-dimensional vertically resolved pysical-biological model. These two regions are the Rhodes cyclonic gyre of the Northern Levantine Sea known to be a major, persistent sub-basin scale feature of the Eastern Mediterranean between the Rhodes and Cyprus Islands, and the anticyclonic gyre of the western Ionian Sea extending meridionally to the east of the Sicily Straits. In the Rhodes basin, the water column below the seasonal thermocline is typically characterized by relatively cold, saline and dense waters. On the contrary, the western anticyclonic Ionian gyre possesses very limited surface-intermediate water interactions because of the presence of less saline Modified Atlantic Waters (MAW) within the upper 100 m layer. The strong stratification introduced by the presence of MAW and LIW underneath prevents deep penetration of the vertical convection and, subsequently, the nutrient supply from deeper levels. Because of these two contrasting dynamical regimes, the two basins reveal quite different vertical nutrient structures, and subsequently quite different biological production characteristics. The annual primary production is estimated as 97.4 gC m^{-2} yr^{-1} in the Rhodes basin. On the other hand, the primary production in the western Ionian Sea amounts only 10% of the Rhodes' case. Therefore, these two basins represent biologically two end members of the Eastern Mediterranean. The annual production cycle also differs slightly in these two basins. The Rhodes gyre possesses a classical production cycle consisting of a strong early spring bloom, a weaker early winter bloom and subsurface production during the summer. In the western Ionian basin, these two blooms are merged with each other to form a long lasting, gradually evolving winter bloom starting from the begining of January to the end of March. The early spring bloom of the Rhodes gyre, on the other hand, has a shorter lifetime, grows and decays exponentially.

Acknowledgements

E.Napolitano greatfully acknowledges the support provided by the Universita' di Messina and Istituto Universitario Navale Environmental Marine Sciences Joint Ph.D Program as a visiting fellow at MIT. P. Malanotte-Rizzoli and T. Oguz acknowledge the NSF support OCE-9633145.

References

Antoine, D., A. Morel, J-M Andre (1995) Algal pigment distribution and primary production in the Eastern Mediterranean as derived from coastal zone color scanner observations. J. Geophys. Res., 100, 16193-16209.

Berland, R.B., A.G. Benzhitski, Z.P. Burlakova, L.V. Georgieva, M.A. Izmestieva, V.I. Kholodov, S.Y. Maestrini (1998) Hydrological structure and particulate matter distribution in Mediterranean seawater during summer. Ocean. Acta, 9, Pelagic Mediterranean Oceanography, 163-177.

Brasseur, P., J.M. Beckers, J.M. Brankart, R. Schoenauen (1996) Seasonal temperature and salinity fields in the Mediterranean Sea: Climatological analyses of a historical data set. Deep-Sea Res.I, 43, 159-192.

Civitarese, G., A. Crise, G. Crispi, R. Mosetti (1996) Circulation effects on nitrogen dynamics in the Ionian Sea. Ocean. Acta, 19, 609-622.

Crise, A., G. Crispi and E. Mauri (1998, in press) A seasonal three-dimensional study of the nitrogen cycle in the Mediterranean Sea. Part I: Model implementation and numerical results. J. Mar. Sys.

Crispi, G., A. Crise, A., E. Mauri (1998, in press) A seasonal three-dimensional study of the nitrogen cycle in the Mediterranean Sea. Part II: Verification of the energy constrained trophic model. J. Mar. Sys.

Doney, S.C., D.M. Glover, R.G. Najjar (1996) A new coupled one dimensional biological-physical model for the upper ocean: applications to the JGOFS Bermuda Time Series Study (BATS) site. Deep-Sea Res., 43, 591-624.

Ediger, D. (1995) Interrelationships among primary production, chlorophyll and environmental conditions in the northern Levantine basin. Ph.D thesis, Middle East Technical University, Institute of Marine Sciences, Erdemli, Icel, Turkey, 187 pp.

Ediger, D. and A. Yilmaz (1996) Characteristics of deep chlorophyll maximum in the northeastern Mediterranean with respect to environmental conditions. J. Mar. Sys., 9, 291-303.

Ediger, D., S. Tugrul, C.S. Polat, A. Yilmaz, I. Salihoglu (1998, in press) Abundance and elemental composition of particulate matter in the upper layer of the northeastern Mediterranean. J. Mar. Syst.

Fasham, M.J.R., H.W. Ducklow, S.M. McKelvie (1990) A nitrogen-based model of plankton dynamics in the oceanic mixed layer. J. Mar. Res., 48, 591-639.

Jassby, A.D. and T. Platt (1976) Mathematical formulation of the relationship between photosynthesis and light for phytoplankton. Limnol. Oceanogr., 21, 540-547.

Levy, M., L. Memery, J-M, Andre (1998) Simulation of primary production and export fluxes in the northwestern Mediterranean Sea. J. Mar. Res., 56, 197-238.

Kuhn, W., and G. Radach (1997) A one dimensional physical-biological model study of the pelagic nitrogen cycling during the spring bloom in the northern North Sea (FLEX'76). J. Mar. Res., 55, 687-734.

Malanotte-Rizzoli, P., B. Manca, M. Ribera, A. theocharis, A. Bergamasco, D. Bregant, G. Budillon, G. Civitarese, D. Georgopoulos, A. Michelato, E. Sansone, P. Scarazzato, E. Souvermezoglou (1997) A synthesis of the Ionian Sea hydrography, circulation and water mass pathways during POEM-Phase I. Prog. Oceanog., 39, 153-204.

May, P.W. (1982) Climatological heat flux estimates of the Mediterranean Sea, Part I: winds and wind stresses. Report 54, NORDA, NSTL Station, 7539529, 56 pp.

McClain, C.R., K. Arrigo, K-S. Tai, D. Turk (1996) Observations and simulations of physical and biological processes at ocean weather station P, 1951-1980. J. Geophys. Res.

McGullicuddy, D.J., J.J. McCarthy, A.R. Robinson (1995) Coupled physical and biological modeling of the spring bloom in the North Atlantic: I. Model formulation and one dimensional bloom processes. Deep-sea Res., 42, 1313-1357.

Oguz, T., H. Ducklow, P. Malanotte-Rizzoli, S. Tugrul, N. Nezlin, U. Unluata (1996) Simulation of annual plankton productivity cycle in the Black Sea by a one-dimensional physical-biological model. J. Geophysical Research, 101, 16585-16599.

Ozsoy, E., A. Hect, U. Unluata, S. Brenner, T. Oguz, J. Bishop, M.A. Latif, Z. Rosentraub (1991) A review of the Levantine Basin circulation and its variability

during 1985-1988. Dyn.Atmos. Oceans, 15, 421-456.

Ozsoy, E., A. Hect, U. Unluata, S. Brenner, H.I. Sur, J. Bishop, T. Oguz, Z. Rosentraub, M.A. Latif (1993) A synthesis of the Levantine Basin circulation and hydrography, Deep-Sea Res., 40, 1075-1119.

Rabitti, S., F. Bianchi, A. Boldrin, L.Daros, G. Socal, C. Totti (1994) Particulate matter and phytoplankton in the Ionian Sea. Ocean. Acta, 17, 297-307.

Robinson, A.R., D. J. McGillicuddy, J. Calman, H. W. Ducklow, M.J.R. Fasham, F.E. Hoge, W.G. Leslie, J.J. McCarthy, S. Podewski, D.L. Porter, G. Saure, J.A. Yoder (1993) Mesoscale and upper ocean variabilities during the 1989 JGOFS bloom study. Deep-Sea Res.II, 40, 9-35.

Salihoglu, I., C. Saydam, O. Basturk, K. Yilmaz, D. Gocmen, E. Hatipoglu, A. Yilmaz (1990) Transport and distribution of nutrients and chlorophyll-a by mesoscale eddies in the northeastern Mediterranean. Mar. Chem., 29, 375-390.

Sur, H.I., E. Ozsoy, U.Unluata (1993) Simultaneous deep and intermediate depth convection in the Northern Levantine Sea, winter 1992. Oceanol. Acta, 16, 33-433.

Yilmaz, A., D. ediger, O. Basturk, S. Tugrul (1994) Phytoplankton fluorescence and deep chlorophyll maxima in the northeastern Mediterranean. Oceanol. acta, 17, 69-77.

Yilmaz, A. and S. Tugrul (1998, in press) The effect of cold- and warm-core eddies on the distribution and stoichiometry of dissolved nutrients in the northeastern Mediterranean. J. Mar. Sys.

PLANKTON CHARACTER
LEVANTINE SEAS

I.SIOKOU-FRAN
K.PAGOU
National Centre for
Ag.Kosmas, Hellini

1.Introduction

The Eastern Mediterranean
characterized by a subtropi
species [1] and therefore its
Ionian and Levantine Seas
continental shelf. The main
Water, the Ionian Surface W
Mediterranean Deep Water
Levantine Sea along with th
in two distinct parts: (a) the
deep troughs and receives E
the Cyclades plateau follow
with the Ionian and the Lev
Cretan Arc respectively.

Several cyclonic
influencing the distributio
oligotrophic [6, 7]. Deep
external inputs to the su
depends on the transportati

Many studies on p
and Levantine Seas were p
9]. Synoptic cruises were
MAST) and national proj
methods, facilitating the
Mediterranean Sea. The pr
data.

P. Malanotte-Rizzoli and V.N. Er
The Eastern Mediterranean as a